Colloids and Surfaces B: Biointerfaces 227 (2023) 113341

Contents lists available at ScienceDirect

Colloids and Surfaces B: Biointerfaces

journal homepage: www.elsevier.com/locate/colsurfb

Engineering phosphatidylinositol-4,5-bisphosphate model membranes enriched in endocytic cargo: A neutron reflectometry, AFM and QCM-D structural study

Daniel Pereira [a,b,1], Andreas Santamaria [b,c,1,2], Nisha Pawar [d], Javier Carrascosa-Tejedor [b,e], Mariana Sardo [a], Luís Mafra [a], Eduardo Guzmán [c,f], David J. Owen [g], Nathan R. Zaccai [g], Armando Maestro [d,h,*], Ildefonso Marín-Montesinos [a,**]

[a] Department of Chemistry, CICECO, University of Aveiro, 3810-193 Aveiro, Portugal
[b] Large Scale Structures Group, Institut Laue-Langevin, 38042 Cedex 9, Grenoble, France
[c] Departamento de Química Física, Universidad Complutense de Madrid, 28040, Madrid, Spain
[d] Centro de Física de Materiales (CSIC, UPV/EHU) - Materials Physics Center MPC, Paseo Manuel de Lardizabal 5, E-20018 San Sebastián, Spain
[e] Division of Pharmacy and Optometry, University of Manchester, M13 9PT Manchester, UK
[f] Instituto Pluridisciplinar, Universidad Complutense de Madrid, 28040 Madrid, Spain
[g] Cambridge Institute for Medical Research, University of Cambridge, CB22 7QQ Cambridge, UK
[h] IKERBASQUE—Basque Foundation for Science, Plaza Euskadi 5, Bilbao 48009, Spain

ARTICLE INFO

Keywords:
Neutron reflectometry
Quartz crystal microbalance with dissipation monitoring
Membrane biomimetics

ABSTRACT

The combination of in vitro models of biological membranes based on solid-supported lipid bilayers (SLBs) and of surface sensitive techniques, such as neutron reflectometry (NR), atomic force microscopy (AFM) and quartz crystal microbalance with dissipation monitoring (QCM-D), is well suited to provide quantitative information about molecular level interactions and lipid spatial distributions. In this work, cellular plasma membranes have been mimicked by designing complex SLB, containing phosphatidylinositol 4,5-bisphosphate (PtdIns4,5P_2) lipids as well as incorporating synthetic lipo-peptides that simulate the cytoplasmic tails of transmembrane proteins. The QCM-D results revealed that the adsorption and fusion kinetics of PtdIns4,5P_2 are highly dependent of Mg^{2+}. Additionally, it was shown that increasing concentrations of PtdIns4,5P_2 leads to the formation of SLBs with higher homogeneity. The presence of PtdIns4,5P_2 clusters was visualized by AFM. NR provided important insights about the structural organization of the various components within the SLB, highlighting that the leaflet symmetry of these SLBs is broken by the presence of CD4-derived cargo peptides. Finally, we foresee our study to be a starting point for more sophisticated in vitro models of biological membranes with the incorporation of inositol phospholipids and synthetic endocytic motifs.

1. Introduction

The plasma membrane (PM) is a crucial interface between a eukaryotic cell and its surrounding environment. Its role is governed not only by its associated proteins, but also by membrane-specific lipids, such as the phospholipid phosphatidylinositol 4,5-bisphosphate (PtdIns4,5P_2). This phosphoinositide is directly involved in mediating diverse processes such as cell migration and signalling, gating of ion channels, signal transduction as well as membrane and vesicular trafficking [1,2]. In particular, the presence of PtdIns4,5P_2 on the inner leaflet of the PM is essential for clathrin-mediated endocytosis (CME). Its phosphorylated inositol ring mediates the recruitment to the PM of CME adaptor proteins, like CALM and AP2. These adaptor proteins also specifically bind to PM-associated transmembrane proteins (termed

* Corresponding author at: Centro de Física de Materiales (CSIC, UPV/EHU) - Materials Physics Center MPC, Paseo Manuel de Lardizabal 5, E-20018 San Sebastián, Spain.
** Corresponding author.
E-mail addresses: armando.maestro@ehu.eus (A. Maestro), imarin@ua.pt (I. Marín-Montesinos).
[1] Both authors contributed equally to this work.
[2] Current affiliation: Center for Structural Biology (CBS), CNRS, INSERM, Univ Montpellier, Montpellier, France.

https://doi.org/10.1016/j.colsurfb.2023.113341
Received 11 March 2023; Received in revised form 5 May 2023; Accepted 9 May 2023
Available online 10 May 2023

cargos), and drive the formation of clathrin-coated vesicles that transport these cargos to endosomes, the cell's major sorting station [3,4].

The AP2, the adaptor protein complex is able to bind dileucine-based (D/ExxxLL) and tyrosine-based (YxxΦ) cargo motifs, which are both widely found in transmembrane proteins at the PM. Due to their short and unstructured nature, the endocytic motifs' biological function has been investigated by using short synthetic peptides, either in solution, or associated to lipids membranes as lipo-peptides [5–7].

Here, we report an in vitro model of the PM based on solid-supported lipid bilayers (SLBs), deposited onto a solid substrate [8,9] enriched in both PtdIns4,5 P_2 and a lipo-peptide containing the dileucine motif from the T-cell surface antigen protein CD4. The position of the peptide moiety mimicked the anchoring point on the PM by which CME could be initiated. The model SLBs' were characterized by neutron reflectometry (NR), atomic force microscopy (AFM) and quartz-crystal microbalance with dissipation monitoring (QCM-D). These techniques have proven to be powerful methods to study the formation and structural organization of similar model membranes [9–11]. While QCM-D can be used to monitor real time formation of bilayers [11–13] (in variable conditions, e.g. buffer composition [14–16] and temperature [17]) and its interaction with proteins [18,19], small molecules [20,21] and even DNA [22,23], NR can be used for the structural study of planar biomimetic membranes under physiological conditions with sub-nanometric resolution in the direction perpendicular to the plane of the membrane [9,24]. In addition, AFM is very useful to visualize the in-plane surface coverage as well as the lipids distribution on the solid/liquid interface [25].

Given the importance of PtdIns4,5P_2 docking sites for protein recruitment, and the likely influence of the CD4 on membrane-protein interactions, we focus here in several key aspects of PtdIns4,5P_2-SLBs

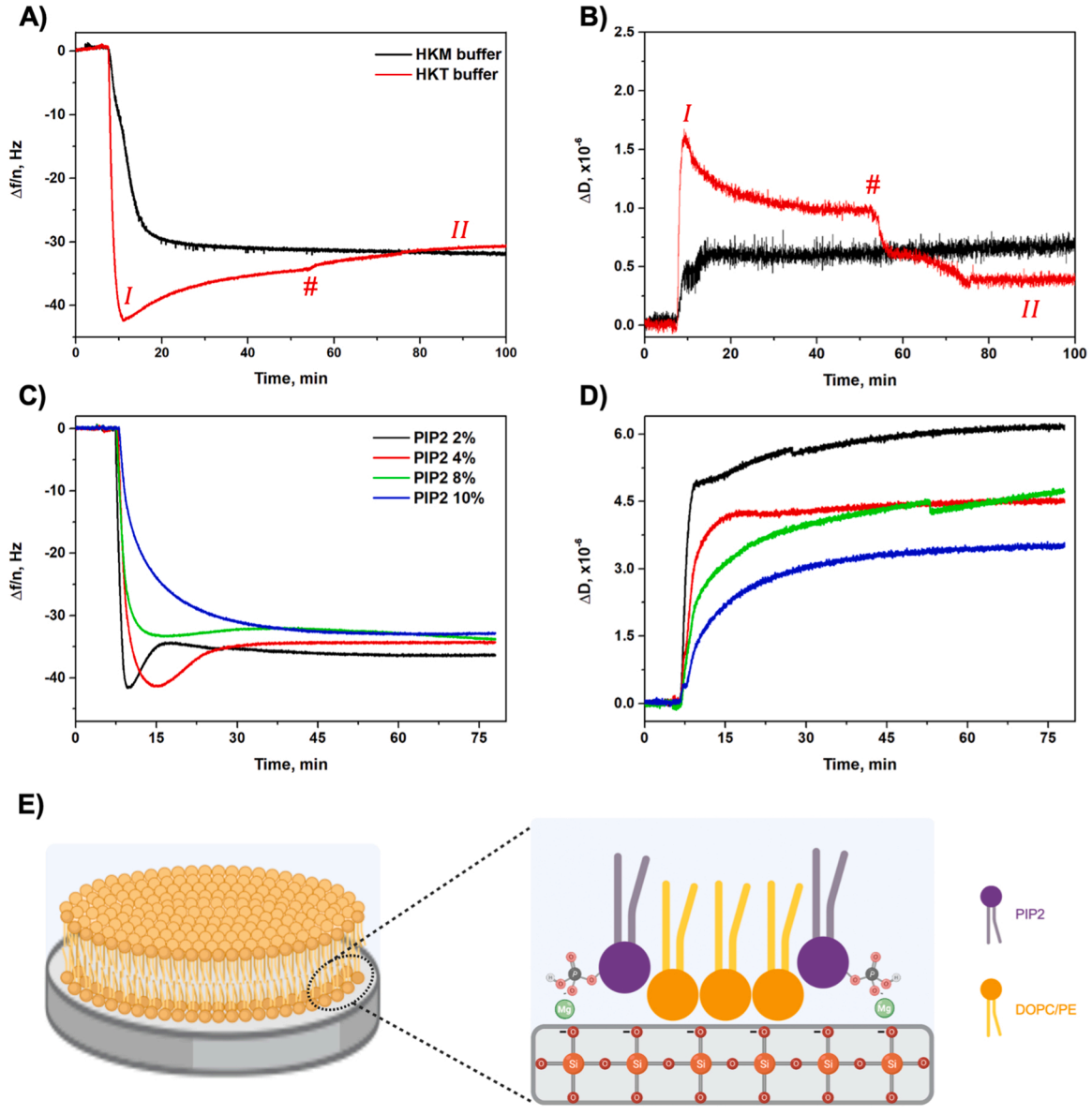

Fig. 1. : Vesicle adsorption and fusion kinetics: frequency shift (A) and dissipation shift (B) plots corresponding to the 3rd overtone (n = 3) for lipid vesicles composed of DOPC, DOPE and PtdIns4,5 P_2 (in molar ratio 7:2:1), prepared with HKM (5 mM Mg^{2+}, black line) and HKT buffer (red line). The different steps of the adsorption and fusion kinetics are indicated with symbols in the panels (***I*** indicates the minimum corresponding to the initial vesicle adsorption, and ***II*** indicates the equilibration of the adsorption and fusion kinetics. # indicates the start of the rinsing with water); panels (C) and (D) show the frequency shifts and dissipation shifts, respectively, corresponding to the 3rd overtone for the adsorption of lipid vesicles containing variable molar percentages of PtdIns4,5 P_2 in HKM buffer. A schematic representation of the charge bridging mechanism mediated by Mg^{2+} is shown in panel (E). The frequency shifts presented in panels (A) and (C) were normalized by the overtone number. The overtones n = 3,5,7,9, and 11 are presented in Fig. S1.

formation such as the fusion kinetic dependence on both the presence of divalent cations interacting with the inositol ring and the concentration of PtdIns4,5P_2. Further analysis of the NR, AFM and QCM-D data, help to elucidate the SLBs structure and composition perpendicular to the plane of the membrane, as well as their mechanical properties. Finally, the coplanarity found for CD4 poly-peptide random chains and the phosphoinositol rings was discussed in terms of a plausible electrostatic interaction between both components.

2. Results and discussion

2.1. Effect of divalent cations on vesicle adsorption and fusion kinetics of PtdIns4,5P_2 enriched SLBs

The formation of SLBs, by liposome adsorption and fusion onto a solid substrate, is highly sensitive to experimental conditions. Vesicle size and concentration, lipid composition, the buffer pH, ionic type and strength, temperature and substrate type influence both the adsorption and fusion mechanisms [8,11]. The adsorption and fusion kinetics of (7:2:1) DOPC:DOPE:PtdIns4,5P_2 liposomes were analyzed by QCM-D (see Methods for liposomes preparation and characterization).

The time evolution of the frequency (Δf/n, where n is the overtone number) and dissipation (ΔD) shifts, for the 3rd overtone (n = 3), monitored during the formation of the SLBs on the substrate surface are reported in Fig. 1A, B. The additional overtones are reported in Fig. S1.

Since the phosphorylated inositol ring of PtdIns4,5P_2 is able to bind intracellular divalent cations, the effect of Mg^{2+} on the SLBs formation by vesicles fusion was determined by comparing the effect of HKT buffer (25 mM HEPES pH 7.2, 125 mM potassium acetate, 1 mM DTT), and of HKM buffer, which is HKT buffer supplemented with 5 mM magnesium acetate (see Methods for further details) (Fig. 1A, B). An electrostatic, divalent ion-mediated clustering mechanism for PtdIns4,5P_2 has been demonstrated both by experimental and theoretical (atomistic molecular dynamics simulations) studies of biomimetic model membranes [26–28].

Independently of the presence of Mg^{2+}, the interaction of the vesicles with the substrate surface yields a decrease of Δf together with the increase of ΔD. This is a clear signature of the adsorption of vesicles on the crystal surface [11]. However, this process of adsorption and rupture of vesicles appears to be Mg^{2+}-dependent, resulting in different profiles when Mg^{2+} is present or not, emphasizing the crucial role of electrostatic interactions in SLB formation. In the absence of Mg^{2+}, the interaction of the vesicles in HKT with the crystal leads to an initial sharp decrease of Δf/n reaching a minimum around t = 10 min (identified by the symbol ***I***), followed by its monotonous increase up to a value of − 30 Hz. Similar dependence was found for the ΔD, which evidences an initial sharp increase reaching a maximum around t = 10 min (***I***), followed by a monotonous decrease until reaching a constant value over time (***II***). These results are compatible with the well-known two-step mechanism of adsorption and fusion of unilamellar lipid vesicles to form SLBs [11]. Thus, the process can be interpreted considering an initial adsorption of the vesicles until a critical surface coverage is reached (characterized by a minimum on Δf and a maximum on ΔD curves in Fig. 1A, B and Fig. S1), followed by vesicle rupture and fusion, giving rise to the formation of planar SLBs (Fig. 1A, B and Fig. S1). The deformation observed in the ΔD curve (Fig. 1B), at t = 50 min (identified by the symbol #), depicts the start of the washing step with the corresponding buffer solution. This step is used to remove any unfused vesicles from the QCM-D microfluid chamber and, therefore, allowing a better stabilization of the system.

Alternatively, in the presence of 5 mM Mg^{2+}, the interaction of the vesicles with the silicon dioxide surface is characterized by a monotonous decrease of the Δf and an increase of the ΔD. This is reminiscent from a situation characterized by a faster fusion of the vesicles upon their strong electrostatic interactions with the silicon dioxide (SiO_2)-coated quartz surface as observed in cationic vesicles such as 1,2-dioleoyl-3-trimethylammonium-propane (DOTAP), for example [29]. Importantly, our results highlight the role of the divalent cation Mg^{2+} as a fusogenic agent, leading to faster adsorption and fusion kinetics. Similar observations were previously reported for SLBs with different lipid compositions, where the fusogenic effect induced by the divalent cation was proven to be ion-dependent [14,15]. The fusogenic character of divalent cations is associated with its role in the mediation of vesicle-substrate interactions by charge bridging (see Fig. 1 **E**). The Mg^{2+} cations are therefore able to mediate charge-bridges between the negatively charged PtdIns4,5 P_2 lipids (zeta potential, $\zeta = -8 \pm 1$ mV; Fig. S8) and the negatively charged surface of the SiO_2-coated quartz sensor [30]. It should be noted that even though the mechanisms of SLB formation in the presence and absence of Mg^{2+} are intrinsically different, the final values of Δf and ΔD are similar, suggesting that the obtained SLBs present similar structure and mechanical properties independently of the formation pathway. In a recent study [29], a similar electrostatic dependence in the mechanism of SLBs formation was observed playing with vesicles surface charge. On one side, zwitterionic DOPC vesicles exhibited a similar two-step mechanism of SLB formation, for which DOPC SLBs requires a critical number of vesicles adsorbed on the SiO_2 sensor surface, as reflected in the minimum in the Δf/n signal (maximum in ΔD), followed by fusion and rupture of vesicles. On the other side, using positively charged, DOTAP vesicles Δf/n steadily decreases until reaching a plateau (similarly to our vesicles in presence of Mg^{2+}) attributed to a strong electrostatic interaction between the positively charged vesicles and the negatively charged SiO_2 surface. Besides, Luchini et al. studied a similar system where vesicles comprised by POPC and 1,2-dioleoyl-sn-glycero-3-phospho-(1′-myo-inositol-3′,4′,5′-trisphosphate), $DOPIP_3$, were studied by QCM-D and NR [31]. The values of Δf obtained are comparable to those reported in this work, however the ΔD values are remarkably smaller than those shown here. This difference might be attributed to different factors: (i) The inclusion of PE lipids in our system, characterized by large negative curvatures [32]. In fact, a recent work demonstrated the formation of POPG-POPE SLBs with full coverage [33]. The QCM-D analysis of this system yielded high ΔD values and spreading of overtones [33]. These characteristics, also observed in the present study, are hallmarks of non-rigid films and are likely induced by the presence of PE lipids although it is usually attributed to the presence of defects and inhomogeneities in simple, single component SLBs [29]. In our case, NR results (see below) confirms the absence of defects in the samples studied. (ii) The presence of PtdIns4,5 P_2 lipids is well known to form submicrometer-sized clusters in SLBs [26,27]. In our case, it is confirmed by AFM images (Fig. 4A). This heterogeneous structure in the plane of the SLBs might be also to induce overtones spreading. Although similar studies have been already performed for POPC [14] and DOPC [15] vesicles, no studies have been reported for DOPC/DOPE lipid mixtures, and vesicles containing PtdIns4,5 P_2 lipids. Nevertheless, it is expected that other divalent ions (e.g. Ca^{2+}, Sr^{2+}) might induce similar effects, as previously demonstrated in analogous systems [14,15], however such analysis was not carried out as it is outside the scope of this work.

2.2. Effect of PtdIns4,5P_2 concentration in the fusion process: monotonic vs two step fusion

The results reported above suggest that the anionic character of PtdIns4,5 P_2 plays a central role on the Mg^{2+}-mediated fusion of lipid vesicles. To obtain a deeper understanding of this, the interaction of vesicles containing DOPC, DOPE and variable molar percentages of PtdIns4,5 P_2 (see Table S1) with the negatively charged sensor surface was studied by QCM-D experiments. Fig. 1C, D show the effect of PtdIns4,5 P_2 concentration on the Δf and ΔD during the formation of bilayers as result of the fusion of vesicles containing DOPC, DOPE and variable amounts of PtdIns4,5 P_2. Even though the variable composition of the unilamellar lipid vesicles does not have any effect on the ability of the vesicles to form SLBs upon interaction with the negatively charged

surface of the sensor, the mechanism of the bilayer formation is dependent on the molar percentage of PtdIns4,5 P_2. Our results suggest that when low concentration of PtdIns4,5 P_2 (2% and 4%) is used, the formation of the SLB follows a two-step mechanism of adsorption and fusion, as demonstrated in the previous section. First, a critical number of vesicles adsorbed on the SiO_2 is reached (minimum in the Δf/n signal and maximum in ΔD), after which the vesicles start to fuse and rupture (increase in the Δf/n signal and decrease in ΔD) until a final continuous SLB is formed (plateau of Δf/n and ΔD signals). For higher concentrations of PtdIns4,5 P_2 (8% and 10%), a spontaneous rupture takes place when the vesicles are adsorbed into the SiO_2 sensor, which can be shown by the monotonous decrease of the Δf/n signal (and increase of the ΔD) until reaching a plateau. This monotonous change of the Δf and ΔD indicates that vesicles with high PtdIns4,5 P_2 loadings fuse immediately upon contact with the silicon substrate. This confirms the important role that the anionic phosphorylated inositol headgroup of PtdIns4,5 P_2 plays in the interaction with cations, such as Mg^{2+}, in the adsorption behavior and fusion kinetics of lipid vesicles. This observation is in agreement with previous studies [34]. In fact, strong electrostatic contributions can favor an instantaneous vesicles fusion without requiring a minimal critical coverage of the surface [35]. Furthermore, the PtdIns4,5 P_2 content is linked to the final properties of the SLB as highlighted by the increase of the absolute value of the Δf and the ΔD (see Fig. 1C, D and Fig. S2). This may be explained in terms of the charge-bridging contributions, which affect both the kinetics of SLB formation and the homogeneity of the final bilayer structure. High concentrations of PtdIns4,5 P_2 induce strong attractive interactions between vesicles and substrate, causing local deformations in the vesicles and reducing their confinement within the bilayer structure, leading to a more uniform homogeneous bilayer. This may be understood considering that for highly charged vesicles (e.g., 10% PtdIns4,5 P_2 characterized by $\zeta = -8 \pm 1$ mV) it is not required a critical coverage for starting their rupture. Moreover, if the fusion process is slowed down, for example when PtdIns4,5 P_2 content is reduced, slightly more laterally heterogenous bilayer are formed, as suggested by the increased spreading of the overtones and higher values of ΔD (Fig. S2). This might be explained by the existence of weaker attractive interactions of the liposomes (rationalized by the lower charge density due to lower concentration of PtdIns4,5 P_2) with the silicon substrate leading to the presence of defects within the SLB, e.g., lipid patches with exposed edges, contributing to energy dissipation and, therefore, large overtone spreading. In fact, it has been demonstrated that defects within the SLB, such as unruptured vesicles and/or lipid patches with exposed edges, contribute to energy dissipation and, therefore, large overtone spreading [29]. Such scenario is expected to be more prominent in vesicles with lower PtdIns4,5 P_2 loadings, where the vesicles lower charge density results in weaker attractive interactions between vesicles and substrate, consequently leading to higher probably of including defects within SLB continuum. This hypothesis agrees with the changes reported in the QCM-D parameters i.e. higher absolute values of Δf and ΔD observed as the PtdIns4,5 P_2 concentration decreases (Fig. 1C, D and Fig. S2). The former parameter (Δf) is related to the formation of thicker films, whereas the increase of the ΔD is indicative of the heterogeneity of the films. Indeed, the in-plane and perpendicular heterogeneities of the formed bilayers are expected to oscillate with an associated delay compared to the homogenous bilayers. Thus, a non-rigid behaviour is expected, which is characterized by increased values of ΔD and spreading of the overtones, as observed in Fig. 1C, D and Fig. S2.

2.3. SLBs with lipid/peptide conjugates as mimics of protein membrane receptors: deposition and structure by QCM-D

The main goal of this work is to design SLBs incorporating peptides mimicking the cytoplasmic ligands from transmembrane proteins. To this end, CD4 lipid-peptide conjugate was included within the lipid mixture used for the preparation of unilamellar vesicles and studied by QCM-D (see Table S1 for compositions and Methods for vesicle preparation). Fig. 2 displays the time dependence of the Δf and ΔD for the adsorption, and subsequent fusion of vesicles including CD4 lipid-peptide conjugate in the presence and absence of PtdIns4,5P_2, as obtained in the HKM buffer.

The presence of PtdIns4,5P_2 emerges as a very important contribution to the final characteristic of the obtained SLBs. In fact, the magnitude of the Δf and ΔD are smaller in the presence of PtdIns4,5P_2 for the liposomes containing the CD4 lipid-peptide conjugate. This may be interpreted by considering that the electrostatic contributions associated with presence of PtdIns4,5P_2 favours the fusion of the unilamellar vesicles due to the interaction with Mg^{2+}, thus leading to the formation of a more homogeneous SLB. This is supported by smaller values of Δf, which is also an indication of a smaller average thickness of the SLB, associated with a reduced probability of the imbibition of intact vesicles with the lipid bilayer. In addition, the time evolutions of the ΔD and overtone spreading also confirm the higher heterogeneity of the bilayers obtained in the absence of PtdIns4,5P_2 (Fig. 2 and Fig. S3). The non-monotonous change of the ΔD with time in absence of PtdIns4,5P_2 suggests a more complex mechanism of SLB formation. This description agrees with the evolution of the ΔD versus Δf/n plots displayed in Fig. S4 for the formation of different composition SLBs. Thus, while for SLBs with PtdIns4,5P_2 in the absence and presence of CD4, the ΔD increases quasi-monotonously as the adsorption proceeds (defined in terms of the decrease of the Δf), in the absence of PtdIns4,5P_2, the evolution of the corresponding ΔD versus Δf/n plot (see Fig. S1) is not monotonous, suggesting a possible initial adsorption of intact vesicles on which the latter are fused as indicated by the presence of a minimum in the curve. Based on our results, it is therefore clear that PtdIns4,5P_2 plays an important role on the formation of SLBs.

After being deposited, the structure and mechanical properties of the SLBs deposited on the surface of the quartz sensor were calculated by the Voigt-Voinova viscoelastic model [36] (see Methods for further details). This is necessary because the Sauerbrey equation that linearly relates Δf with material deposited onto the crystal is no longer valid for the studied bilayers due to their non-rigid character [37–39]. Therefore, the validity of the Voinova-Voigt for describing the behavior of the obtained bilayers is supported in two conditions: (i) the non-rigid character of lipid bilayers, evidenced by the spread of the frequency shifts corresponding to the different measured overtones and the relatively high changes of the dissipation factor, which is mostly due to the distribution of the water molecules surrounding the polar head-groups (confirmed by **NR**, see next section), results in frictional (viscous) contributions and crystal oscillation dampening, and (ii) the spatial arrangement of the lipid bilayers observed by AFM images (Fig. 4) which confirms the homogenous 3D organization of the bilayers, allowing us to consider them as a single layer undergoing a delayed displacement in relation to the quartz crystal [40].

The thickness and mechanical properties of SLBs with the previous mentioned compositions (DOPC:DOPE:PtdIns4,5P_2, DOPC:DOPE:CD4 and DOPC:DOPE:PtdIns4,5P_2:CD4), calculated through the Voigt-Voinova model (using the stabilized regions after buffer wash, Fig. S5), are reported in Fig. 3. The resulting bilayer thickness was plotted in panel **A**, elastic shear modulus (μ_f) in **B**, shear viscosity (η_f) in **C**, and relaxation time ($\tau_f = \eta_f/\mu_f$) in **D**, which provides a ratio between the different contributions to the viscoelastic response.

As expected, differences in the parameters are observed depending on the specific lipid compositions. In the case of SLBs composed of DOPC, DOPE and PtdIns4,5 P_2 with or without CD4, the thickness in the order of 40–60 Å is similar to a typical DOPC bilayer (see Fig. 3A) [41–45]. However, in absence of PtdIns4,5P_2, there is a ~1.5 fold increase in thickness for a SLB containing CD4, thereby suggesting the peptide protrudes from the SLB. Furthermore, the peptide embedded in the lower leaflet of the SLB increase the spacing between the sensor surface and the bilayer. Surprisingly, when PtdIns4,5 P_2 is combined

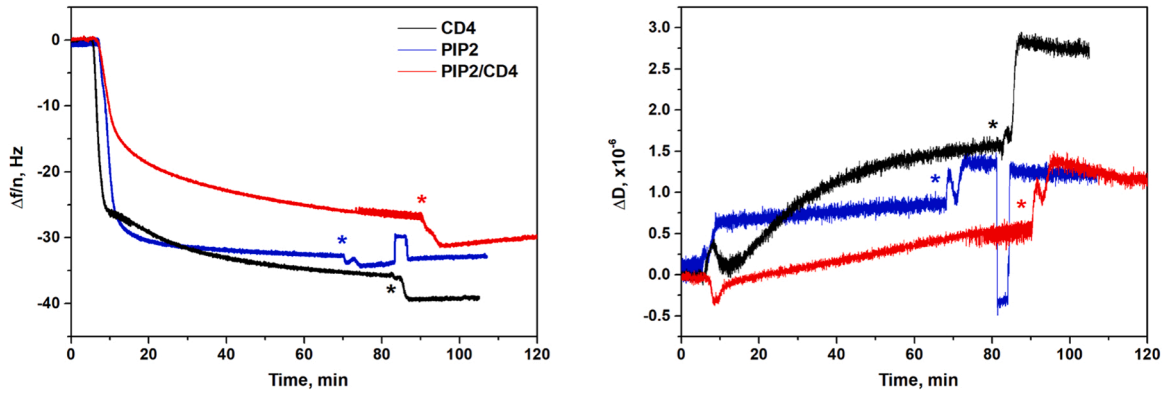

Fig. 2. : Vesicle adsorption and fusion kinetics: frequency shift (A) and dissipation shift (B) plots corresponding to the 3rd overtone for unilamellar lipid vesicles composed of DOPC, DOPE and the CD4 lipid-conjugate in presence and absence of PtdIns4,5 P_2. Experiments were performed in HKM buffer. The frequency shifts presented in panel (A) were normalized by the overtone number. * highlights the start of washing step.

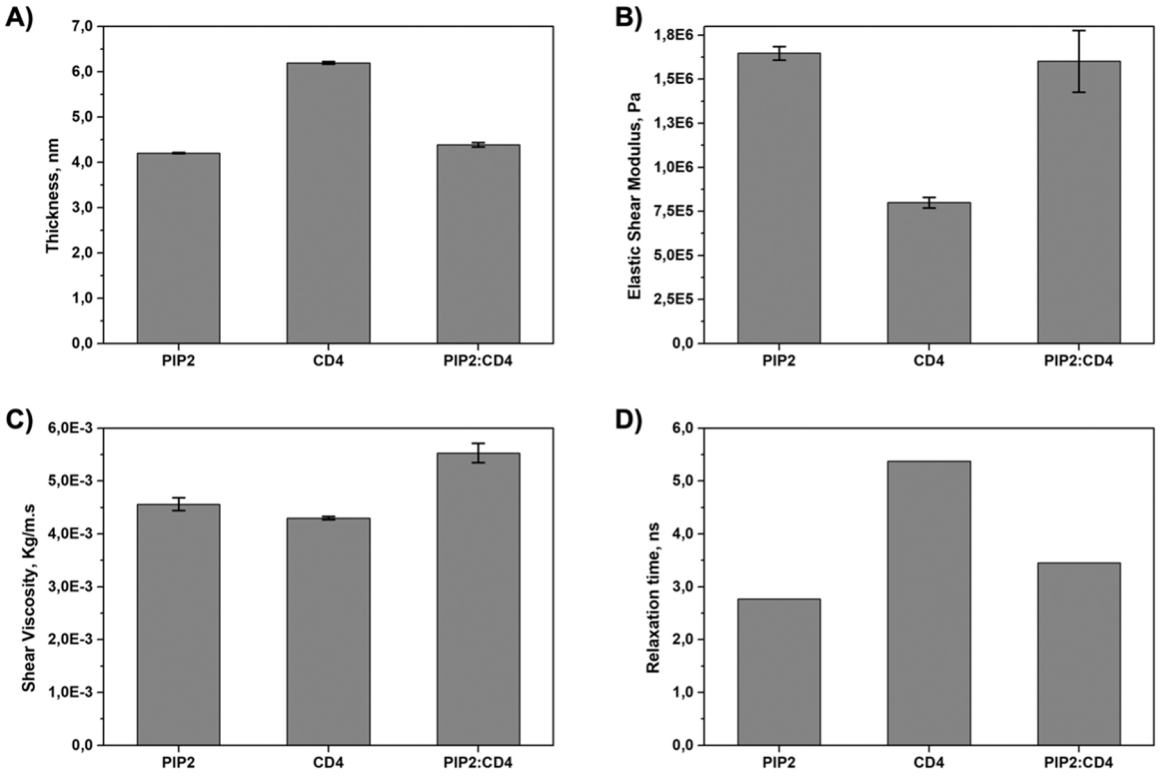

Fig. 3. : Properties of SLBs obtained from QCM-D analysis. The parameters were extracted by using the Voigt-Voinova viscoelastic model. (A) Thickness. (B) Elastic shear modulus. (C) Shear viscosity. (D) Relaxation time.

with CD4 in the SLB, a different scenario is observed. Although it was expected that the presence of CD4 lipid-peptide conjugate within the SLB would increase the average SLB thickness in comparison to a bilayer composed solely of lipids, this behavior was only observed when the CD4 was embedded in the PM in the absence of PtdIns4,5 P_2. Curiously, the simultaneous insertion of CD4 lipid-peptide conjugate and PtdIns4,5 P_2 in the SLB resulted in a reduction of the average thickness of the film. This effect can be explained considering the electrostatic attraction between the CD4 polypeptide chain, hypothesized as a random coil chain bearing a total net positive charge, and the negatively charged headgroup of PtdIns4,5 P_2. In fact, the inclusion of CD4 results in a slightly decrease of the zeta potential of PtdIns4,5 P_2 enriched liposomes (from $\zeta = -8 \pm 1$ to -7 ± 1 mV; Fig. S8). As a result of this electrostatic interaction CD4 is placed at the level of the lipid headgroups, as demonstrated by NR in the next section, and, as a consequence, preventing its polypeptide chains to protrude towards the bulk phase (See scheme in Fig. 5G). Besides, AFM images reported in Fig. 4 also shown how the electrostatic interaction of CD4 with PtdIns4,5P_2 gives rise to a reduction in the lipid phase demixing by decreasing the number of PtdIns4,5P_2 clusters.

Similarly, to the variability in the thickness of the SLBs, the mechanical properties were also found to be dependent on the lipid composition and the presence of CD4. In the absence of CD4, the values of shear elasticity modulus and viscosity are in good agreement with previous reports for SLBs composed of POPC [40]. The incorporation of CD4 into the bilayers increases the shear viscosity and, therefore, the viscoelastic relaxation time in a manner strongly dependent on SLB specific composition. In the presence of CD4 and no PtdIns4,5P_2, the relaxation time is ~1.5-folds higher than that corresponding to bilayers with both PtdIns4,5P_2 and CD4, and ~2-folds higher than that of

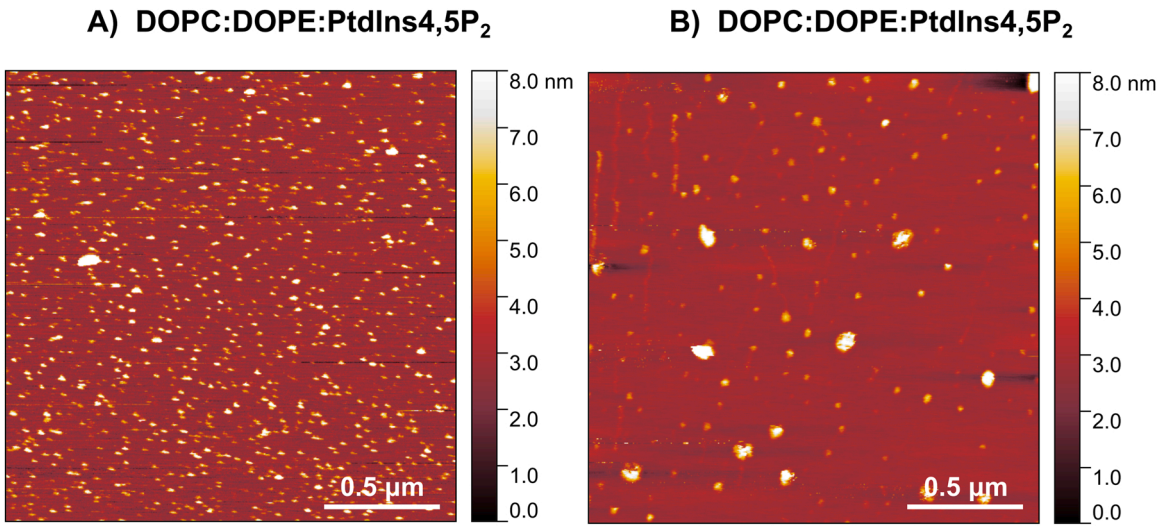

Fig. 4. : Membrane phase demixing and PtdIns4,5P2 clusterization is also dependent on the presence of CD4. SLBs composed by DOPC:DOPE:PtdIns4,5P2 (A) and DOPC:DOPE:PtdIns4,5P2:CD4 (B) in HKM buffer are examined by fluid-phase peak force tapping mode AFM. Scale bars are 0.5 µm.

bilayers with PtdIns4,5P_2 and without CD4. This reflects the higher resistance to motion in the former SLB due to the bilayer strong heterogeneity character.

2.4. Further determination of the SLBs structure by Neutron Reflectometry

NR elucidates the structure and composition of SLBs in the direction perpendicular to the plane of the membrane with sub-nanometric resolution. A 1D profile of the reflectivity (R), defined as the ratio of neutrons reflected from the interface over the incident intensity of the neutron beam, is measured in specular conditions as a function of the momentum transfer vector normal to the interface, $Q_z = 4\pi \sin\theta / \lambda$, where θ is the angle of incidence and λ is the wavelength of the neutron beam.

Here, SLBs composed of DOPC:DOPE:PtdIns4,5P_2 and also enriched in CD4 dileucine motifs were found to be laterally homogeneous on the length scale of the in-plane neutron coherence length, on the order of several microns [46]. This implies that the measured R(Q_z) profile can be linked with an in-plane averaged scattering length density (SLD) depth profile across the membrane delimited by this coherence length and, therefore, the structure of the membrane can be determined as a function of the distance from the silicon substrate surface. The goal was to elucidate the structural differences of the SLBs due to the presence of the CD4 short, random coil peptide. By simultaneously fitting NR profiles measured in 4 isotopic contrasts, the position of the CD4 peptide was determined in the direction perpendicular to the plane of the membrane with emphasis on the evaluation and molar quantification of CD4 peptide asymmetric distribution in between leaflets. The isotopic contrasts used in the experiments consisted of HEPES-NaCl buffer prepared in (1) pure D_2O, (2) pure H_2O, (3) silicon-matched water (SiMW), which is a mixture of D_2O:H_2O that contrast match the SLD of the silicon crystal (2.07 10^{-6} A^{-2}), and (4) air contrast-matched water (ACMW), which is characterized by an SLD= 0.

NR data of PtdIns4,5P_2 containing SLBs, in the absence of CD4, were fitted with a model (illustrated in Fig. 5G) consisting of 5 layers defining the lipid bilayer, including both inner and outer leaflets, a wetting layer of water between the inner lipid leaflet and the native SiO_2 layer, that naturally grows on silicon substrates whose thickness was determined prior to the bilayer deposition (see Table S3). Each layer was characterized by a thickness, an interfacial roughness, an in-plane average SLD and an averaged molecular volume of the molecular components (see Tables S2 and S3 and Fig. 5G for a scheme of the model). The NR profiles were fitted in each contrast buffer as shown by the good agreement between the fitting curves and the experimental reflectivity data plotted as RQ_z [4] vs Q_z (to emphasize the fine details of the modeling at high Q_z values) in Fig. 5A. The bilayer was modelled considering two layers for inner and outer lipid headgroups and one intermediate layer defining the aliphatic tails region (layers 4 and 5, Fig. 4 SLB w/PIP2, are considered as one layer), which is formed by two identical lipid leaflet acyl tails, yielding a thickness of 30 Å and a water content of 4%, thus confirming high lipid coverage. Moreover, a water layer of 4 Å between the bilayer and the silicon crystal was also considered. The resulting SLD profiles for each contrast are reported in Fig. 5 B. From the SLD distribution as a function of the distance to the silicon substrate, the variation of the volume fraction profiles of each layer was calculated using the difference of two error functions (see **Methods**) and plotted in Fig. 5C. The area-per-molecule (APM) obtained was ~70 $Å^2$ and the total thickness was found to be 46 Å in agreement with QCM data (see Fig. 3 A) and similar systems studied in the literature [31,47].

In the presence of CD4 (NR profiles shown in Fig. 5 D), the bilayer resulted in an asymmetrical structure composed by two lipid leaflet acyl tails with different thickness: 13 Å the outer, in contact with the bulk phase and 17 Å the corresponding to the inner leaflet in contact with the solid support. The total size of the bilayer, calculated through a 6-layer model, resulted in 48 Å, again in agreement with QCM data (see Fig. 3 A). An increase of the thickness of the inner headgroup was observed with respect to the sample in absence of CD4, together with a decrease of the water content (see Fig. 5C, F). The higher percentage of CD4 conjugate in the inner leaflet increase both tails and headgroups layer thickness. Regarding the headgroups, this is due to the presence of the peptide, which also reduces the water volume fraction. In addition, although the lipid conjugated to CD4 (Fig. S3) contains 16-carbon atoms acyl chains, against the 18-carbon atoms chains of DOPC and DOPE lipids, its presence increases the orientation order of the hydrocarbon tails giving rise to a remarkable increase in the thickness. These facts together make an asymmetric APM distribution per leaflet (see Table S2). Finally, as already obtained from the analysis of QCM-D experimental data, the values of thickness for the two PtdIns4,5P_2-containing bilayers, with and without CD4, are similar, thus confirming that the random coil peptide prefers laying on the bilayer, rather than extending away from it, being attracted by the PtdIns4,5P_2 negative charges. The formation of enriched PtdIns4,5P_2 SLBs with an asymmetric, quantifiable presence of lipo-peptides containing the dileucine motif from the T-cell surface antigen protein CD4, can open an avenue to the rational design of complex peptide/lipid biomimetic membranes

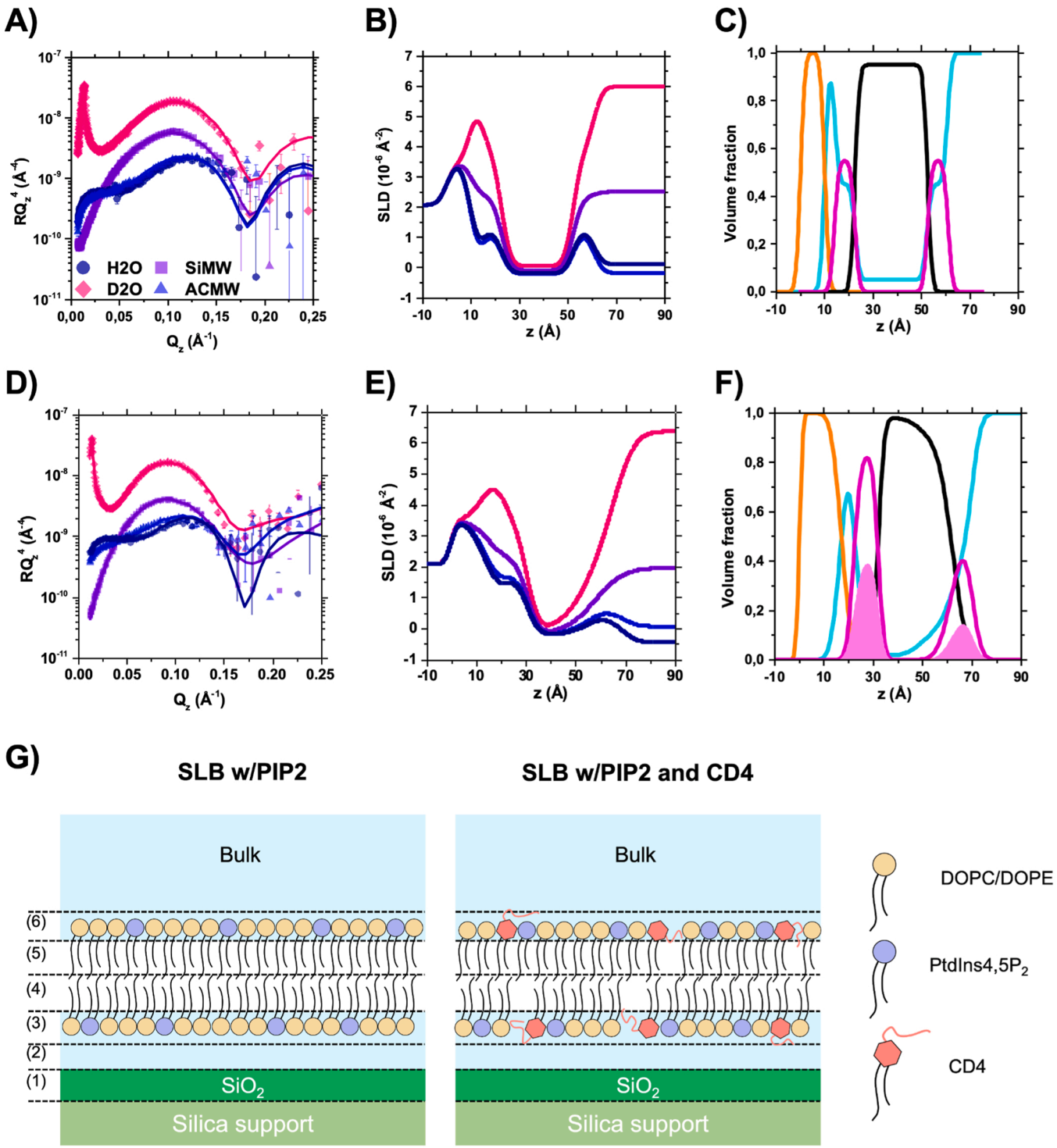

Fig. 5. : Reflectivity profiles of (A) DOPC:DOPE:PtdIns4,5P_2 (70:20:10) and (D) DOPC:DOPE:PtdIns4,5P_2:CD4 (66.5:20:10:3.5) in the 4 contrasts: H_2O (dark blue circle), ACMW (blue triangles), SiMW (violet squares) and D_2O (pink diamonds). The relative fits are presented as lines. (B) and (E) show the SLD profiles perpendicular to the interface of DOPC:DOPE:PtdIns4,5P_2 (70:20:10) and DOPC:DOPE:PtdIns4,5P_2:CD4 (66.5:20:10:3.5)respectively: H_2O (dark blue line), ACMW (blue line), SiMW (violet line) and D_2O (pink line). (C) and (F) report the volume fraction profiles perpendicular to the interface, showing the contribution of silicon oxide (orange line), aliphatic tails (black line), hydrophilic headgroups (magenta), and water (cyan line). The volume fraction related to CD4 peptide moiety is shown as light pink area in (F). (G) Schematic representation of the SLB surface after incorporation of PtdIns4,5P_2 lipids (shown as purple circles) and in the presence and absence of the lipid-peptide conjugate CD4 (shown as salmon hexagon). The NR fitted parameters for the layers 1–6 can be found in Table S2.

analysed not only by QCM-D and NR but also by other surface sensitive techniques [9,48] and solid-state NMR [49,50], therefore providing complementary information for a broader understanding of these type of systems.

3. Conclusion

An in vitro model based on SLBs composed of DOPC:DOPE: PtdIns4,5 P_2 and enriched in CD4 dileucine lipo-peptide conjugates was studied by a combination of NR, AFM and QCM-D techniques. The effect

of Mg^{2+} on SLB formation indicates that divalent cations can mediate the interaction between the negatively charged PtdIns4,5 P_2-containing liposomes and QCM-D sensor surface promoting a faster adsorption and fusion kinetics. In addition, increasing amounts of PtdIns4,5 P_2 were screened to determine how its anionic character influences vesicle adsorption, fusion kinetics and SLBs formation. Higher levels of PtdIns4,5 P_2 in the SLBs were crucial for the creation of homogenous SLBs. These also affected the mechanism of formation showing a transition from a single to a two-step process in the time scale of the QCM-D experiments. Overall, this multi-technique approach combining NR, AFM and QCM-D provided results regarding the mechanical properties as well as out-of-plane structure of the SLBs in the presence and absence of lipo-peptide conjugate CD4.

In conclusion, this work will contribute towards a better design of in vitro model systems based on SLBs that incorporate peptides as mimics of protein ligands. The interaction between PtdIns4,5 P_2 and CD4 lipo-peptides might have a direct influence on membrane curvature, modulating the binding of different peripherical membrane proteins which are fundamental events in the initiation of the CME pathway.

4. Materials and methods

4.1. Materials

The lipids (see Figs. S6), 1,2-dioleoyl-sn-glycero-3-phosphocholine (DOPC, ≥ 99,0% purity), 1,2-dioleoyl-sn-glycero-3-phosphoethanolamine (DOPE, ≥ 99,0% purity) and L-α-phosphatidylinositol-4,5-bisphosphate (ammonium salt) (PtdIns4,5P_2, ≥ 99,0% purity) were supplied by Avanti Polar Lipids Inc. (Alabaster, USA) and used without further purification. CD4 peptide was covalently linked to the synthetic lipid 16:0 MPB PE, 1,2-Dipalmitoyl-sn-Glycero-3-Phosphoethanolamine-N-[4-(p-maleimidophenyl) butyramide]. A detailed description of the synthesis process of the lipid-peptide conjugates can be found in the work by Höning et al. [6].

The experiments were performed in HKM buffer pH = 7.2, whose composition is the following: 25 mM HEPES (4-(2-hydroxyethyl)piperazine-1-ethanesulfonic acid and N-(2-hydroxyethyl)piperazine-N′-(2-ethanesulfonic acid)), 125 mM potassium acetate, 5 mM magnesium acetate, and 1 mM DTT (threo-1,4-dimercapto-2,3-butanediol). HEPES (in solution (1 M in H_2O) and powder (≥ 99.5% purity)), potassium acetate (≥ 99,0% purity), magnesium acetate (≥ 99,0% purity), and DTT (≥ 99,0% purity) were purchased from Sigma Aldrich (Saint Louis, MO, USA). An analogous version of this buffer, named HKT buffer, was prepared following the same composition without adding magnesium acetate.

The phospholipid solutions were prepared by dissolving the lipid powder (DOPC, DOPE and PtdIns4,5P_2) in chloroform until a final concentration of 1.0 mg·mL^{-1}. All the solutions were then stored on the freezer, at a temperature below − 20 ºC, until further use. Ultra-pure water was generated by passing deionized water through a Milli-Q unit (total organic content=4 ppb; resistivity=18 MΩ·cm, Milli-Q, Merck KGaA, Darmstadt, Germany).

4.2. Vesicle preparation

The phospholipid and CD4 solutions, previously dissolved in chloroform, were mixed according to the desired composition, inside glass vials. The molecular ratios used for the different components are shown in Table S1. The volatile solvent was evaporated under a continuous stream of argon, and then the glass vials were left under vacuum overnight to ensure evaporation of any remaining solvent.

In order to obtain samples suitable for QCM-D measurements, the resulting lipid films (sample from #1 to #4, Table S1) were re-hydrated with a mixture of buffer:water (in volume ratio of 8:2, respectively) up to a final lipid concentration of 0.1 mg·mL^{-1}. The samples were left overnight at room temperature with end-over-end rotation. The multilamellar vesicles formed after hydration were then subjected to a series of treatments (freeze-thaw, tip sonication and extrusion) to convert them into unilamellar vesicles (Fig. S7 and Table S4). First, the vesicles were subjected to 5–10 successive freeze-thaw cycles with liquid nitrogen and ice, then tip sonicated (Sonopuls HD 2200, Bandelin, Germany), with a titanium probe (MS73 with microtip of 3 mm), for 15–20 min, with repeated on/off pulses of 2 s and 3 s, respectively, and power amplitude of 20%. Finally, the vesicle dispersions were manually extruded using a commercial mini extruder kit (Avanti Polar Lipids, AL, Alabaster, USA) assembled with polycarbonate membranes (Whatman Inc., Clifton, NJ, USA) of 100 nm pore size. The extrusion cycles were repeated 15–25 times and the obtained dispersions of vesicles were stored at 4 °C until experiment. The size of the unilamellar lipid vesicles was monitored through dynamic light scattering (Zetasizer Nano ZS90, Malvern Instruments, U.K.), before injection into the QCM-D. The measurements were performed with temperature-control set at 20 ºC and the scattering angle at 90º, showing the formation of lipid vesicles with monodisperse size distributions and diameter close to 100 nm (Table S5). The zeta potential of the vesicles, ζ, was obtained from measurements of electrophoretic mobility (μ_e) by Laser Doppler velocimetry performed also in the Zetasizer Nano ZS90. The measured values of μ_e were transformed into ζ values using Henry's relationship assuming the liposomes fulfill the Smoluchowski's limit [51]. The accuracy in the determination of ζ *was better than* ± 5 mV.

To produce SLBs for NR experiments, the lipid films (samples #2 and #4, Table S1) were re-hydrated at room temperature in HEPES 5 mM, NaCl 150 mM, $MgCl_2$ 3 mM buffer, up to 1 mg·mL^{-1} lipid concentration, and vortexed to fully suspend vesicles. Immediately before use, the suspensions were tip sonicated for 5 min at pulses of 1 s on/off.

4.3. QCM-D measurements

QCM-D experiments were performed using a commercial Q-Sense E4 instrument (Q-Sense, Biolin Scientific AB, Göteborg, Sweden) fitted with SiO_2-coated AT-cut quartz sensors (QSX 303, Q-Sense, Biolin Scientific AB, Göteborg, Sweden). These sensors were thoroughly cleaned, prior to their use, in an ultrasound bath by sequential immersion in chloroform, acetone, ethanol and water. Afterwards, the cleaned sensors were dried under a gentle stream of nitrogen and exposed to UV-ozone cleaning in a ProCleaner™ Plus instrument (BioForce Nanosciences, Virginia Beach, VI, USA) for 30 min. The crystals were then immersed in water and dried under a gentle stream of nitrogen. The cleaned and hydrophilized crystals were immediately fitted inside the QCM-D flow module. The flow module was then connected to a peristaltic pump (Multichannel Peristaltic Pump IPC-N 4, Ismatec, Switzerland) operating with a fixed flow rate of 0.10 mL·min^{-1}.

QCM-D measures the impedance spectra of the quartz crystal for the fundamental frequency (f = 5 MHz) and odd overtones up to the 13th. Before the experiments, the fundamental frequencies of the overtones were recorded up to the equilibration of the signal at the experimental temperature (20 ºC), which is evidenced for a stable baseline, i.e., the Δf and ΔD remaining constant for at least 5 min. After equilibration in buffer, the lipid vesicles dispersion (0.10 mg·mL^{-1}) is introduced in the flow cell and left under incubation for 20–40 min, allowing the adsorption and fusion processes. The measurements were performed using freshly prepared vesicles that were stored at a temperature of 4ºC for a maximum of ~ 12 h (overnight).

The QCM-D allows monitoring, simultaneously, the changes of the Δf and ΔD over time. The QCM-D data were analysed using the software Q-Tools (version 3.0.10, Q-Sense, Biolin Scientific AB, Göteborg, Sweden), which is based in the model proposed by Voinova et al. [36]. This procedure makes it possible to correlate the changes in the resonant frequency and dissipation factor of the different overtones with physical parameters of the layers (thickness t_j, density ρ_j, elasticity μ_j and viscosity η_j), according to the following two equations (Note: *The fundamental frequency is not used for data analysis due to the noisy character of its*

signal):

$$\Delta f \approx -\frac{1}{2\pi\rho_q t_q}\left\{\frac{\eta_l}{\delta_l}+\sum_{f=1,2}\left[t_f\rho_f\omega-2t_f\left(\frac{\eta_l}{\delta_l}\right)^2\frac{\eta_f\omega^2}{\mu_f^2+\omega^2\eta_f^2}\right]\right\} \quad (1)$$

$$\Delta D \approx \frac{1}{2\pi f\rho_q t_q}\left\{\frac{\eta_l}{\delta_l}+\sum_{f=1,2}\left[2t_f\left(\frac{\eta_l}{\delta_l}\right)^2\frac{\mu_f\omega}{\mu_f^2+\omega^2\eta_f^2}\right]\right\} \quad (2)$$

where ρ_q and t_q are the density and thickness of the quartz crystal sensor, η_l and δ_l are the density of the liquid and viscous penetration depth of the shear wave in the bulk liquid, ω is the angular frequency of the oscillation [36,52,53]. For the fitting of experimental data, the fluid density and viscosity were fixed at 1.0×10^3 kg·m^{-3} and 1.0×10^{-3} kg·m^{-1}·s^{-1}, respectively, as all experiments were conducted in aqueous dispersions. The density of the lipid bilayer was fixed at 1.1×10^3 kg·m^{-3}, which is consistent with previous studies [11].

4.4. Neutron reflectometry data acquisition

Neutron Reflectometry experiments were performed on the time-of-flight horizontal reflectometer FIGARO at the Institut Laue-Langevin (ILL), Grenoble (France) [54]. Two different angles of incidence ($\theta = 0.8°$ and 3.2°) and a wavelength resolution of 7% $d\lambda/\lambda$ were used, yielding a momentum transfer of 7×10^{-3} Å^{-1} < Q_z < 0.26 Å^{-1}, normal to the interface.

The data were reduced and normalized to a measurement of pure D_2O using COSMOS [55]. Custom-made solid/liquid flow cells with polished silicon crystals (111) with a surface area of 5×8 cm^2 were used. Neutron cell flow modules and O-rings were cleaned by bath sonication in a Decon90 solution, then in pure water and finally in ethanol. The crystals were cleaned by bath sonication in chloroform, acetone, ethanol and water. Finally, the crystals were dried with nitrogen flux and treated with Plasma cleaner for 2 min before neutron cell assembly. During the measurements, the temperature was maintained constant by circulating water from a thermostatic water bath. Variation of the aqueous solvent contrast was achieved by exchanging the bulk solvent using a HPLC pump set to a flow rate of 2 mL·min^{-1}. After characterization of bare silicon substrate, the dispersion of lipid vesicles was injected by a syringe and incubate for 10 min, followed by a washing step with pure water to allow SLB formation. The SLB was characterized in 4 different isotopic solvent contrasts: H_2O (SLD = $-0.56\bullet10^{-6}$ Å^{-2}), ACMW (91.9:8.1 *v/v* % H_2O:D_2O, SLD = 0), Silicon matched water (SiMW, 62:38 *v/v* % H_2O:D_2O, SLD = $2.07\bullet10^{-6}$ Å^{-2}) and D_2O (SLD = $6.36\bullet10^{-6}$ Å^{-2}). Each of the above-mentioned contrasts includes HEPES 5 mM, NaCl 150 mM buffer (without $MgCl_2$).

4.5. Neutron reflectometry data modeling

Modelling of the NR data has been done by approximating the continuous bilayer structure perpendicular to the plane of the membrane using a model composed of N layers of varying scattering length density (SLD) and thickness (t) modulated by a roughness (σ) parameter, which describes the interfacial mixing of the layers, as follows:

$$\mathrm{SLD}(z) = \sum_{i=0}^{N}\frac{SLD_i - SLD_{i-1}}{2}\left(1+erf\left(\frac{z-t_i}{\sigma_i\sqrt{2}}\right)\right) \quad (3)$$

The data analysis was performed using MOTOFIT software [56]. For PtdIns4,5 P_2-containing bilayer (no CD4), a symmetric bilayer model was used, that is a 5-layer model, characterized by two polar headgroups-layers and a unique hydrophobic tails-layer, which includes the tails from both lipid leaflets, a water layer between bilayer and crystal, and a Silicon oxide layer (SLD = 3.47 10^{-6} Å^{-2}). For PtdIns4, 5 P_2-CD4-containing bilayer, an asymmetric model was used, in which each tail leaflet was described by a layer, leading to a 6-layer model. Indeed, the lipid composition in the two leaflets was found to be different, being the inner leaflet (i.e., the one closer to the silicon substrate) richer in peptide than the outer one. The fixed parameters used in the fitting procedure (see Table S2) are the scattering length densities of heads (SLD_{heads}) and tails (SLD_{tails}), as well as the molecular volumes (V_{heads} and V_{tails}). Besides, the exchange of labile protons was considered for the calculation of SLD_{heads}. The thickness of tails (t_{tails}) and headgroups (t_{heads}) layer, as well as their water content (f_{tails} and f_{heads}), were considered as fitting parameters (see Table S3), together with the roughness of each layer. The water volume fraction in the headgroups-layers was constrained to ensure same area-per-molecule (APM) of lipid headgroups and tails, in each layer, $APM = V_i/t_i f_i$ (with i = aliphatic tails or headgroups). Experimental data of SLB in the four solvent contrasts were fitted together. Thus, the ambiguity in the interpretation of the sample structure, which may arise from the different sensitivity that the curves exhibit with respect to the different sample components, is significantly reduced.

4.6. Atomic force microscopy

Supported lipid bilayers were formed on freshly cleaved mica surface (discs with 12 mm of diameter). 50 µL of 1 mg/mL vesicle solution were added on the mica and the sample was placed in a closed petri dish and left to incubate for 30 min at room temperature. Later, the sample was washed 4 times with water to remove unfused vesicles and the SLBs formed were imaged in the presence of buffer in the AFM liquid cell. All images were obtained with a multimode AFM and a Nanoscope V controller (Bruker). The AFM was operated in Peak Force mode in liquid, at room temperature. The Silicon tip on Silicon Nitride Cantilever (Model: PFQNE-AL), with a spring constant 0.8 N/m and a resonant frequency 300 kHz, were used for scanning. The images were taken at a scan rate of 1 Hz and 512 × 512 pixels. The images were acquired with the Nanoscope Software. They were topologically flattened and analyzed by using NanoScope Analysis 1.90 software (Bruker) and Gwyddion software (version 2.60).

CRediT authorship contribution statement

Daniel Pereira: Conceptualization, Methodology, Investigation, Data curation, Writing – Original Draft, Visualization. **Andreas Santamaria:** Conceptualization, Methodology, Investigation, Data curation, Writing – Original Draft, Visualization. **Nisha Pawar:** Methodology, Investigation, Data curation, Visualization. **Javier Carrascosa-Tejedor:** Methodology, Investigation, Writing – Review & Editing. **Mariana Sardo:** Writing – Review & Editing. **Luís Mafra:** Writing – Review & Editing. **Eduardo Gúzman:** Resources, Writing – Review & Editing, Supervision. **David J. Owen:** Resources, Writing – Review & Editing. **Nathan R. Zaccai:** Resources, Writing – Review & Editing, Supervision. **Armando Maestro:** Conceptualization, Methodology, Resources, Writing – Review & Editing, Supervision, Project Administration, Funding Acquisition. **Ildefonso Marín-Montesinos:** Conceptualization, Methodology, Resources, Writing – Review & Editing, Supervision, Project Administration, Funding Acquisition.

Declaration of Competing Interest

The authors declare that they have no known competing financial interests or personal relationships that could have appeared to influence the work reported in this paper.

Data Availability

Data will be made available on request.

Acknowledgments

The authors thank the Institut Laue-Langevin for the allocation of

beamtime and the Partnership for Soft Condensed Matter (PSCM) for the lab support. E.G. and A.M. acknowledge the financial support from MICINN under grants PID2019-106557GB-C21 and PID2021-129054NA-I00, respectively. A.M. also acknowledges the financial support received from the IKUR Strategy under the collaboration agreement between Ikerbasque Foundation and Materials Physics Center on behalf of the Department of Education of the Basque Government. I.M.-M. acknowledges the EMBO organization for the EMBO Short-Term Fellowship 8740. D.J.O and N.Z acknowledge financial support from the Wellcome Trust (grant 207455/Z/17/Z) awarded to D.J.O. This work was developed within the scope of the project CICECO-Aveiro Institute of Materials, UIDB/50011/2020 and UIDP/50011/2020, financed by national funds through the Portuguese Foundation for Science and Technology/MCTES.

Conflicts of interest

The authors declare no conflict of interest. The funders had no role in the design of the study; in the collection, analyses, or interpretation of data; in the writing of the manuscript, or in the decision to publish the results.

Appendix A. Supporting information

Supplementary data associated with this article can be found in the online version at doi:10.1016/j.colsurfb.2023.113341.

References

[1] G. Di Paolo, P. De Camilli, Phosphoinositides in cell regulation and membrane dynamics, Nature 443 (2006) 651–657.
[2] T.K. Phan, et al., Phosphoinositides: multipurpose cellular lipids with emerging roles in cell death, Cell Death Differ. 26 (2019) 781–793.
[3] G.R.V. Hammond, et al., PI4P and PI(4,5)P2 are essential but independent lipid determinants of membrane identity, Science 337 (2012) 727–730, 80.
[4] T.F.J. Martin, PI(4,5)P2 regulation of surface membrane traffic, Curr. Opin. Cell Biol. 13 (2001) 493–499.
[5] D.J. Owen, P.R. Evans, A structural explanation for the recognition of tyrosine-based endocytotic signals, Sci. (80-.) 282 (1998) 1327–1332.
[6] S. Höning, et al., Phosphatidylinositol-(4,5)-bisphosphate regulates sorting signal recognition by the clathrin-associated adaptor complex AP2, Mol. Cell 18 (2005) 519–531.
[7] B.T. Kelly, et al., A structural explanation for the binding of endocytic dileucine motifs by the AP2 complex, Nature 456 (2008) 976–979.
[8] G.J. Hardy, R. Nayak, S. Zauscher, Model cell membranes: Techniques to form complex biomimetic supported lipid bilayers via vesicle fusion, Curr. Opin. Colloid Interface Sci. 18 (2013) 448–458.
[9] L.A. Clifton, et al., Design and use of model membranes to study biomolecular interactions using complementary surface-sensitive techniques, Adv. Colloid Interface Sci. 277 (2020), 102118.
[10] M. Eeman, M. Deleu, From biological membranes to biomimetic model membranes. *Biotechnology*, Agron. Soc. Environ. vol. 14 (2010) 719–736.
[11] R.P. Richter, R. Bérat, A.R. Brisson, Formation of solid-supported lipid bilayers: an integrated view, Langmuir 22 (2006) 3497–3505.
[12] T. Viitala, J.T. Hautala, J. Vuorinen, S.K. Wiedmer, Structure of anionic phospholipid coatings on silica by dissipative quartz crystal microbalance, Langmuir 23 (2007) 609–618.
[13] T.H. Anderson, et al., Formation of supported bilayers on silica substrates, Langmuir 25 (2009) 6997–7005.
[14] B. Seantier, B. Kasemo, Influence of mono- and divalent ions on the formation of supported phospholipid bilayers via vesicle adsorption, Langmuir 25 (2009) 5767–5772.
[15] M. Dacic, et al., Influence of divalent cations on deformation and rupture of adsorbed lipid vesicles, Langmuir 32 (2016) 6486–6495.
[16] A. Kunze, F. Zhao, A.-K. Marel, S. Svedhem, B. Kasemo, Ion-mediated changes of supported lipid bilayers and their coupling to the substrate. A case of bilayer slip? Soft Matter 7 (2011) 8582–8591.
[17] E. Reimhult, F. Höök, B. Kasemo, Temperature dependence of formation of a supported phospholipid bilayer from vesicles on SiO2, Phys. Rev. E Stat. Phys. Plasmas Fluids Relat. Interdiscip. Top. 66 (2002) 4.
[18] S. Meker, H. Chin, T.N. Sut, N.-J. Cho, Amyloid-β peptide triggers membrane remodeling in supported lipid bilayers depending on their hydrophobic thickness, Langmuir 34 (2018) 9548–9560.
[19] C. Satriano, et al., Ferritin-supported lipid bilayers for triggering the endothelial cell response, Colloids Surf. B Biointerfaces 149 (2017) 48–55.
[20] X. Fan, et al., Lipid-mimicking peptide decorates erythrocyte membrane for active delivery to engrafted MDA-MB-231 breast tumour, Eur. J. Pharm. Biopharm. 152 (2020) 72–84.
[21] C.M. Bailey-Hytholt, T. Puranik, A. Tripathi, A. Shukla, Investigating interactions of phthalate environmental toxicants with lipid structures, Colloids Surf. B Biointerfaces 190 (2020), 110923.
[22] C. Montis, et al., Nucleolipid bilayers: A quartz crystal microbalance and neutron reflectometry study, Colloids Surf. B Biointerfaces 137 (2016) 203–213.
[23] J.G. Woller, K. Börjesson, S. Svedhem, B. Albinsson, Reversible hybridization of DNA anchored to a lipid membrane via porphyrin, Langmuir 28 (2012) 1944–1953.
[24] G. Fragneto, R. Delhom, L. Joly, E. Scoppola, Neutrons and model membranes: Moving towards complexity, Curr. Opin. Colloid Interface Sci. 38 (2018) 108–121.
[25] F. Dufrêne, Y. Boland, T., W. Schneider, J., R. Barger, W, U. Lee, G, Characterization of the physical properties of model biomembranes at the nanometer scale with the atomic force microscope, Faraday Discuss. 111 (1999) 79–94.
[26] W.G. Ellenbroek, et al., Divalent cation-dependent formation of electrostatic PIP2 clusters in lipid monolayers, Biophys. J. 101 (2011) 2178–2184.
[27] Y.-H. Wang, et al., Divalent cation-induced cluster formation by polyphosphoinositides in model membranes, J. Am. Chem. Soc. 134 (2012) 3387–3395.
[28] E. Bilkova, et al., Calcium directly regulates phosphatidylinositol 4,5-bisphosphate headgroup conformation and recognition, J. Am. Chem. Soc. 139 (2017) 4019–4024.
[29] L. Bar, et al., Interactions of hydrophilic quantum dots with defect-free and defect containing supported lipid membranes, Colloids Surf. B Biointerfaces 210 (2022), 112239.
[30] S.H. Behrens, D.G. Grier, The charge of glass and silica surfaces, J. Chem. Phys. 115 (2001) 6716–6721.
[31] A. Luchini, et al., Towards biomimics of cell membranes: Structural effect of phosphatidylinositol triphosphate (PIP3) on a lipid bilayer, Colloids Surf. B Biointerfaces 173 (2019) 202–209.
[32] J. Jouhet, Importance of the hexagonal lipid phase in biological membrane organization, Front. Plant Sci. 4 (2013).
[33] T.K. Lind, M.W.A. Skoda, M. Cárdenas, Formation and characterization of supported lipid bilayers composed of phosphatidylethanolamine and phosphatidylglycerol by vesicle fusion, a simple but relevant model for bacterial membranes, ACS Omega 4 (2019) 10687–10694.
[34] M.C. Howland, A.W. Szmodis, B. Sanii, A.N. Parikh, Characterization of physical properties of supported phospholipid membranes using imaging ellipsometry at optical wavelengths, Biophys. J. 92 (2007) 1306–1317.
[35] M. N'Diaye, J.-P. Michel, V. Rosilio, Relevance of charges and polymer mechanical stiffness in the mechanism and kinetics of formation of liponanoparticles probed by the supported bilayer model approach, Phys. Chem. Chem. Phys. 21 (2019) 4306–4319.
[36] M.V. Voinova, M. Rodahl, M. Jonson, B. Kasemo, Viscoelastic acoustic response of layered polymer films at fluid-solid interfaces: continuum mechanics approach, Phys. Scr. 59 (1999) 391–396.
[37] Sauerbrey, G.Verwendung von Schwingquarzen zur Wägung dünner Schichten und zur Mikrowägung. Zeitschrift für Phys. 155, 206–222 (1959).
[38] M.C. Dixon, Quartz crystal microbalance with dissipation monitoring: enabling real-time characterization of biological materials and their interactions, J. Biomol. Tech. 19 (2008) 151–158.
[39] A.D. Easley, et al., A practical guide to quartz crystal microbalance with dissipation monitoring of thin polymer films, J. Polym. Sci. 60 (2022) 1090–1107.
[40] N.-J. Cho, K.K. Kanazawa, J.S. Glenn, C.W. Frank, Employing two different quartz crystal microbalance models to study changes in viscoelastic behavior upon transformation of lipid vesicles to a bilayer on a gold surface, Anal. Chem. 79 (2007) 7027–7035.
[41] J. Pan, S. Tristram-Nagle, N. Kučerka, J.F. Nagle, Temperature dependence of structure, bending rigidity, and bilayer interactions of dioleoylphosphatidylcholine bilayers, Biophys. J. 94 (2008) 117–124.
[42] J. Gallová, D. Uhríková, A. Islamov, A. Kuklin, P. Balgavý, Effect of cholesterol on the bilayer thickness in unilamellar extruded DLPC and DOPC liposomes: SANS contrast variation study, Gen. Physiol. Biophys. 23 (2004) 113–128.
[43] Z.V. Leonenko, E. Finot, H. Ma, T.E.S. Dahms, D.T. Cramb, Investigation of temperature-induced phase transitions in DOPC and DPPC phospholipid bilayers using temperature-controlled scanning force microscopy, Biophys. J. 86 (2004) 3783–3793.
[44] S.J. Attwood, Y. Choi, Z. Leonenko, Preparation of DOPC and DPPC supported planar lipid bilayers for atomic force microscopy and atomic force spectroscopy, Int. J. Mol. Sci. 14 (2013) 3514–3539.
[45] M. Orsi, J. Michel, J.W. Essex, Coarse-grain modelling of DMPC and DOPC lipid bilayers, J. Phys. Condens. Matter 22 (2010), 155106.
[46] A. Maestro, P. Gutfreund, In situ determination of the structure and composition of Langmuir monolayers at the air/water interface by neutron and X-ray reflectivity and ellipsometry, Adv. Colloid Interface Sci. 293 (2021), 102434.
[47] A. Santamaria, et al., Strikingly different roles of SARS-CoV-2 fusion peptides uncovered by neutron scattering, J. Am. Chem. Soc. 144 (2022) 2968–2979.
[48] J. Carrascosa-Tejedor, A. Santamaria, D. Pereira, A. Maestro, Structure of DPPC monolayers at the air/buffer interface: a neutron reflectometry and ellipsometry study, Coatings 10 (2020).
[49] B. Bechinger, DNP solid-state NMR of biological membranes, eMagRes (2018) 25–34, https://doi.org/10.1002/9780470034590.emrstm1558.

[50] P.C.A. van der Wel, New applications of solid-state NMR in structural biology, Emerg. Top. life Sci. 2 (2018) 57–67.
[51] T. Tadros, Zeta potential in colloid science. Principles and application, Colloids Surf. 5 (1982) 79–80.
[52] Höök, F. & Kasemo, B. The QCM-D Technique for Probing Biomacromolecular Recognition Reactions BT - Piezoelectric Sensors. in (eds. Janshoff, A. & Steinem, C.) 425–447 (Springer Berlin Heidelberg, 2007). doi:10.1007/978–3-540–36568-6_12.
[53] Liu, G. & Zhang, G. Basic Principles of QCM-D. in (eds. Liu, G. & Zhang, G.) 1–8 (Springer Berlin Heidelberg, 2013). doi:10.1007/978–3-642–39790-5_1.
[54] R. Cubitt, G. Fragneto, D17: the new reflectometer at the ILL, Appl. Phys. A 74 (2002) s329–s331.
[55] P. Gutfreund, et al., Towards generalized data reduction on a chopper-based time-of-flight neutron reflectometer, J. Appl. Crystallogr. 51 (2018) 606–615.
[56] A. Nelson, Co-refinement of multiple-contrast neutron/X-ray reflectivity data using MOTOFIT, J. Appl. Crystallogr. 39 (2006) 273–276.